

Direct Fabrication of a Superconducting Two-Dimensional Electron Gas on $\text{KTaO}_3(111)$ via Mg-Induced Surface Reduction

Chun Sum Brian Pang,^{1,2} Bruce A. Davidson,^{1,2} Fengmiao Li,^{1,2} Mohamed Oudah,^{1,2} Peter C. Moen,^{1,2} Steef Smit,^{1,2} Cissy T. Suen,^{1,2,3} Simon Godin,^{1,2} Sergey A. Gorovikov,⁴ Marta Zonno,⁴ Sergey Zhdanovich,^{1,2} Giorgio Levy,^{1,2} Matteo Michiardi,^{1,2} Alannah M. Hallas,^{1,2} George A. Sawatzky,^{1,2} Robert J. Green,^{1,2,5} Andrea Damascelli,^{1,2} and Ke Zou^{1,2}

¹⁾*Quantum Matter Institute, University of British Columbia, Vancouver, British Columbia V6T 1Z4, Canada*

²⁾*Department of Physics & Astronomy, University of British Columbia, Vancouver, British Columbia V6T 1Z1, Canada*

³⁾*Max Planck Institute for Solid State Research, 70569 Stuttgart, Germany*

⁴⁾*Canadian Light Source, Inc., Saskatoon, Saskatchewan S7N 2V3, Canada*

⁵⁾*Department of Physics & Engineering Physics, University of Saskatchewan, Saskatoon, Saskatchewan S7N 5E2, Canada*

(*Electronic mail: csbpang@phas.ubc.ca, damascelli@physics.ubc.ca, kzou@phas.ubc.ca)

(Dated: 23 December 2025)

Two-dimensional electron gases (2DEGs) at the surfaces of KTaO_3 have become an exciting platform for exploring strong spin-orbit coupling, Rashba physics, and low-carrier-density superconductivity. Yet, a large fraction of reported KTaO_3 -based 2DEGs has been realized through chemically complex overayers that both generate carriers and can obscure the native electronic structure, making spectroscopic access to the underlying 2DEG challenging. Here, we demonstrate a simple and direct method to generate a superconducting 2DEG on $\text{KTaO}_3(111)$ using Mg-induced surface reduction in molecular-beam epitaxy (MBE). Mg has an extremely low sticking coefficient at elevated temperatures, enabling the formation of an ultrathin (<1–2 monolayer) MgO layer that is transparent to soft X-ray photoemission (XPS) and angle-resolved photoemission spectroscopy (ARPES). This allows direct measurement of the surface chemistry and low-energy electronic structure of the pristine reduced surface without the need for a several-nanometer-thick capping layer. XPS shows clear reduction of Ta^{5+} to lower oxidation states, while ARPES reveals a parabolic Ta 5d conduction band with a \sim 150 meV bandwidth and additional subband features arising from quantum confinement. Transport measurements confirm a superconducting transition below 0.6 K. Together, these results demonstrate a chemically straightforward and controllable pathway for fabricating spectroscopically accessible superconducting 2DEGs on $\text{KTaO}_3(111)$, and provide a powerful new platform for investigating the mechanisms underlying orientation-dependent superconductivity in KTaO_3 -based oxide interfaces.

KTaO_3 (KTO) is a wide-gap perovskite insulator ($E_g \approx 3.6$ eV¹) whose surfaces can host two-dimensional electron gases (2DEGs) with remarkable physical properties. Conductive states have been engineered through *in situ* cleaving^{2–4} or by growing overayers such as AlO_x , EuO , LaTiO_3 , and LaVO_3 .^{5–8} These methods induce the formation of oxygen vacancies and/or atomic substitution at potassium sites near the KTO surface.^{6,9,10} Consequently, Ta^{5+} ions are reduced to lower oxidation states such as Ta^{4+} , leading to increased electron occupation in the Ta 5d conduction band and the formation of 2DEGs.^{6,9}

Due to the presence of heavy Ta atoms, KTO exhibits strong spin-orbit coupling of about 0.3 eV, which gives rise to pronounced Rashba spin splitting and enables efficient spin-charge interconversion in KTO-based 2DEGs.^{11–14} Beyond their spintronic functionality, several KTO 2DEGs formed by overlayer growth have also been found to exhibit two-dimensional superconductivity, with the critical temperature (T_c) strongly dependent on crystallographic orientation, reaching up to 2.2 K on KTO(111), 1.3 K on KTO(110), and only 0.25 K on KTO(001).^{6–10,15,16} This orientation-dependent superconductivity is unique to KTO and has not been observed in other materials, with its underlying mechanism remaining a topic of active discussion.^{7,17}

To develop a microscopic understanding of this behavior, it is essential to directly resolve the intrinsic electronic structure of KTO-based 2DEGs under well-controlled conditions. However, many established methods for creating such 2DEGs rely on chemically complex or relatively thick overayers to drive the necessary redox processes. These overayers can obscure the 2DEG from surface-sensitive probes and may introduce structural or chemical perturbations, making it challenging to compare different orientations under identical surface conditions. This motivates the development of alternative approaches that produce a clean, minimally perturbed, and spectroscopically accessible superconducting 2DEG directly at the KTO surface.

Here, we demonstrate that a superconducting 2DEG can be realized on the KTO(111) surface through direct Mg reduction, enabling *in situ* access to both the surface chemistry and low-energy electronic structure via X-ray photoemission spectroscopy (XPS) and angle-resolved photoemission spectroscopy (ARPES). Using molecular beam epitaxy (MBE), we developed a three-stage growth procedure to fabricate an $\text{MgO}/\text{KTO}(111)$ heterostructure that introduces a 2DEG at the KTO(111) surface. Reflection high-energy electron diffraction (RHEED) was employed to monitor the surface structure and guide each stage of the fabrication process.

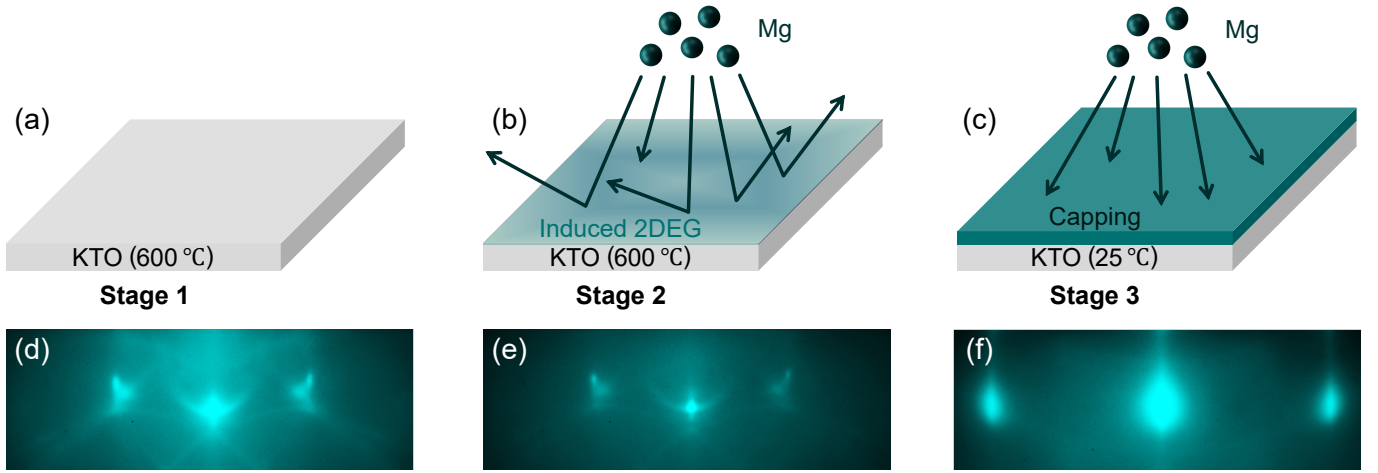


FIG. 1. Fabrication of the MgO/KTO(111) sample. Schematic diagrams of (a) Stage 1, substrate degassing; (b) Stage 2, high-temperature surface reduction using Mg; and (c) Stage 3, room-temperature capping. The corresponding RHEED patterns along the [1-12] direction are shown in (d) to (f).

Stage 1 involves substrate degassing. KTO(111) single-crystal substrates ($10 \times 10 \times 0.5 \text{ mm}^3$, MTI Corporation) were cleaved into $2.5 \times 2.5 \times 0.5 \text{ mm}^3$ pieces using a diamond scribing pen. Each substrate was degassed at $600 \text{ }^\circ\text{C}$ for 1 hour under ultra-high vacuum (UHV) conditions better than $2.0 \times 10^{-8} \text{ Torr}$ [Fig. 1(a)]. The RHEED pattern, which repeats every 60° of sample rotation (not shown) as expected for the KTO(111) surface, remains unchanged during heating and degassing aside from slight blurring [Fig. 1(d)], suggesting the absence of structural reconstruction of the KTO(111) surface at elevated temperatures. The mild reduction in sharpness may be attributed to the formation of defects at high temperature, a behavior previously observed by atomic force microscopy on KTO(001) surfaces cleaved and annealed in UHV.¹⁸

Stage 2 involves the high-temperature surface reduction of the KTO substrate using Mg. The substrate was held at $600 \text{ }^\circ\text{C}$ and exposed to an elemental Mg flux of $2.5 \times 10^{13} \text{ atoms cm}^{-2} \text{ s}^{-1}$ for 12 minutes, with the Mg effusion cell maintained at $310 \text{ }^\circ\text{C}$ [Fig. 1(b)]. Since the substrate temperature is much higher than that of the Mg cell, the incident Mg atoms have a very low sticking coefficient and are largely re-evaporated or scattered upon arrival. Nevertheless, a fraction of the incoming Mg atoms reacts with lattice oxygen to form MgO, which has a much higher sticking coefficient and adsorbs onto the KTO surface as an ultrathin layer or as small clusters. This reaction extracts oxygen from the topmost KTO unit cells, creating oxygen vacancies that drive electron transfer into the Ta 5d conduction bands and reduce surface Ta⁵⁺ ions. As a result, a 2DEG is stabilized at the KTO(111) surface after reduction, and the corresponding RHEED pattern dims but remains visible, with no additional diffraction spots or streaks observed [Fig. 1(e)]. Since the RHEED electron beam probes only the top few atomic layers, the similarity of diffraction patterns before and after reduction indicates that the KTO(111) surface is not significantly obscured by the adsorbed MgO. This suggests that the MgO overlayer is no more than 1–2 monolayers thick (i.e., $< 1 \text{ nm}$), consistent with the

low sticking coefficient of Mg on a hot substrate. Only Mg atoms that react with the KTO surface to form MgO could contribute to film formation; with the resulting ultrathin overlayer, the 2DEG remains highly exposed, allowing direct *in situ* probing of its electronic structure using surface-sensitive techniques such as XPS and ARPES immediately following Stage 2.

Stage 3 involves the growth of a capping layer at room temperature, which can be performed either directly after surface reduction (Stage 2) or following *in situ* XPS and ARPES measurements. The sample was allowed to settle to room temperature, then exposed again to an elemental Mg flux of $2.5 \times 10^{13} \text{ atoms cm}^{-2} \text{ s}^{-1}$ for 12 minutes, with the Mg cell maintained at $310 \text{ }^\circ\text{C}$ [Fig. 1(c)]. At this lower substrate temperature, Mg atoms exhibit a high sticking coefficient and readily deposit on top of the 2DEG, forming an Mg overlayer. Based on the flux and deposition time, the Mg overlayer thickness is estimated to be approximately 4 nm. The RHEED pattern [Fig. 1(f)] transforms into broadened spots with increased spacing, indicative of a rough but crystalline capping layer.¹⁹ The ratio of RHEED spot spacing between Fig. 1(d) and Fig. 1(f) is 0.57:1, matching the inverse ratio of the in-plane lattice constants of KTO(111) (5.62 \AA) and Mg (3.21 \AA). The pattern also repeats every 60° , consistent with the hexagonal close-packed structure of Mg. Upon air exposure, the Mg overlayer oxidizes into MgO, serving as a protective capping layer for *ex situ* transport measurements of the 2DEG.

As a control experiment, the same three-stage fabrication procedure was applied to a sapphire substrate; the sample remains insulating, confirming the absence of a 2DEG and indicating that the Mg capping layer fully oxidizes into MgO. A separate control sample of KTO fabricated without Stage 2 (i.e., without high-temperature Mg exposure) is likewise insulating. These results demonstrate that the electronic properties of the MgO/KTO(111) heterostructure produced by the three-stage approach arise directly from the 2DEG formed at the

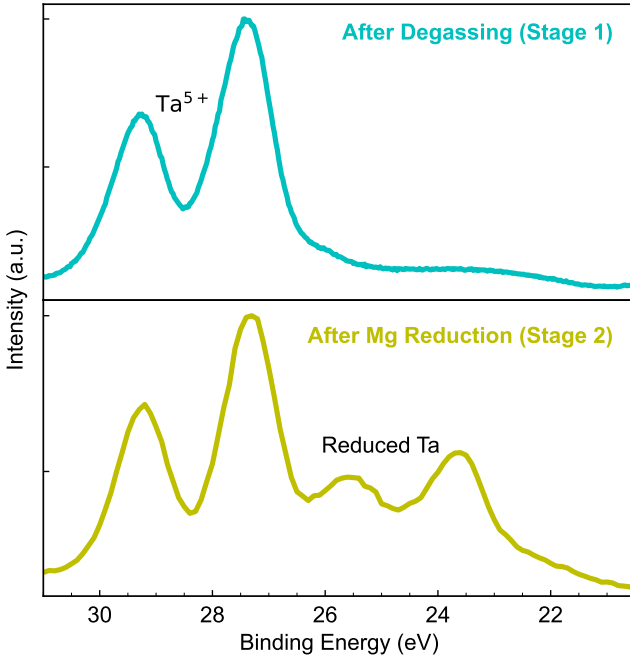


FIG. 2. XPS spectra of an MgO/KTO(111) sample around the 4f core level of Ta. The spectra are taken right after the degassing of KTO(111) substrate (top), and after the surface reduction with Mg (bottom).

reduced KTO(111) surface.

To examine the surface chemistry associated with the Mg treatment, low-energy X-ray photoemission spectroscopy (XPS) measurements were performed at 20 K around the Ta 4f core levels before and after Mg deposition [Fig. 2], using p-polarized 120 eV photons. The emitted photoelectrons have kinetic energies of 80–100 eV and therefore possess inelastic mean free paths of approximately 5 Å,²⁰ making the measurements extremely surface sensitive and probing only the top-most 1–2 monolayers.

After substrate degassing (Stage 1), the surface is dominated by Ta⁵⁺ species, as evidenced by the Ta 4f doublet centered at 27.4 and 29.3 eV [Fig. 2, top],²¹ indicating that the surface remains largely unreduced. In contrast, following the Mg surface treatment (Stage 2), the Ta 4f spectrum displays a pronounced increase in low-binding-energy spectral weight relative to the Ta⁵⁺ doublet [Fig. 2, bottom]. Such an enhancement of reduced Ta components is consistent with electron accumulation at the KTO surface, signaling the formation of a surface 2DEG. This direct spectroscopic signature is a key advantage of our ultrathin-overlayer approach.

To investigate the possible realization of superconductivity induced by Mg reduction, we performed *ex situ* temperature-dependent transport measurements on the MgO/KTO(111) samples [Fig. 3]. Upon cooling below 1 K in zero magnetic field, the resistance shows a sharp drop into a low-resistivity state, reaching zero resistance below 0.3 K. The systematic suppression of the transition temperature under applied magnetic fields further confirms the superconducting nature of this

transition. At zero field, the critical temperature defined at half the normal-state resistance is $T_{c,1/2} = 0.56$ K, lower than the 2.2 K reported by Liu *et al.*¹⁰ This difference likely reflects the lower carrier densities of our samples, consistent with the trends and calculations reported in Ref. 17. Since Mg, MgO, and bulk KTO are all non-superconducting, we conclude that the observed superconductivity originates from the 2DEG formed at the reduced KTO(111) surface.

To probe the electronic structure of the 2DEG in the MgO/KTO(111) system, we performed *in situ* ARPES measurements on the pristine Mg-reduced KTO(111) surface immediately after Stage 2. The resulting Fermi surface [Fig. 4(a)] exhibits a predominantly triangular shape with small protrusions located at the midpoints of the triangle edges. The three corners of the triangle and the three protrusions alternate upon rotation around Γ , and they point toward the M points of the surface Brillouin zone. This pattern is consistent with the star-of-David-like Fermi surfaces reported by Bruno *et al.*²² on free KTO(111) surfaces and by Mallik *et al.*²³ on Eu/KTO(111) 2DEGs. As discussed in Ref. 22, such a star-shaped Fermi surface originates from hybridization among the three Ta 5d t_{2g} orbitals, further supporting that the 2DEG in MgO/KTO(111) is generated through the reduction of surface Ta⁵⁺ ions by Mg.

The corresponding band dispersion along the M– Γ –M direction exhibits a parabolic shape with an occupied bandwidth of approximately 150 meV [Fig. 4(b)]. In addition, a shallow subband-like feature appears near the Γ point and manifests as a central peak in the momentum distribution curve (MDC) at the Fermi level [Fig. 4(b), top]. This feature has been described as a quantum well state—a replica of the main parabolic band arising from quantum confinement of the 2DEG at the KTO surface.^{22,23} The presence of this subband in our dispersion data is therefore consistent with the expected two-dimensional nature of the electronic states at the reduced KTO(111) surface.

In summary, we have demonstrated a simple, direct, and

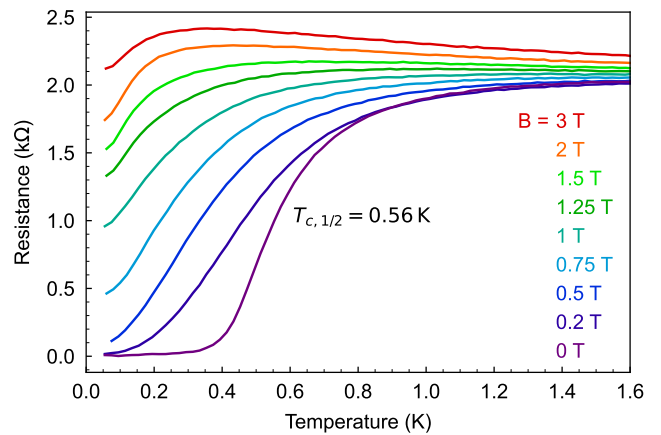


FIG. 3. Low-temperature transport measurements. Resistance as a function of temperature between 60 mK and 1.6 K for out-of-plane magnetic fields ranging from 0 to 3 T. The critical temperature at half the normal-state resistance ($T_{c,1/2}$) is fitted and shown.

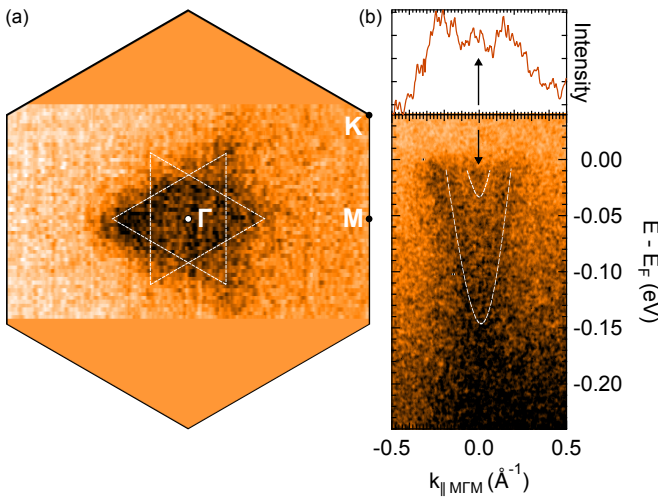


FIG. 4. ARPES data of the Mg-reduced KTO(111) surface. (a) Fermi surface in the first surface Brillouin zone with high-symmetry points labeled. (b) Band dispersion along the M–Γ–M direction, with the momentum distribution curve (MDC, top) at E_F . All data were acquired with p-polarized 105.5 eV photons at 15 K. White dotted lines are included in both the Fermi surface and band-dispersion panels as guides to the eye.

generalizable MBE-based method for generating superconducting 2DEGs on KTO(111) via Mg-induced surface reduction while retaining full *in situ* spectroscopic access. *Ex situ* magnetic-field-dependent transport measurements confirm the superconducting transition to a zero-resistance ground state, and its connection to a confined 2DEG at the Mg-reduced KTO(111) surface is established through the observation of quantum-well subband features in *in situ* ARPES.

This approach can be extended to KTO(110) and KTO(001), enabling direct investigation of the surface chemistry and electronic structure of 2DEGs across different crystallographic orientations. Such studies may provide valuable insight into the origin of the unconventional, orientation-dependent superconductivity observed in KTO-based heterostructures. Moreover, the versatility and simplicity of the Mg-reduction method make it a promising strategy for generating 2DEGs in other insulating oxides, broadening the available toolkit for oxide interface engineering.

This research was undertaken thanks in part to funding from the Max Planck–UBC–UTokyo Centre for Quantum Materials and the Canada First Research Excellence Fund, Quantum Materials and Future Technologies. This project is also funded by the Natural Sciences and Engineering Research Council of Canada (NSERC); the Canada Foundation for Innovation (CFI); the Department of National Defence (DND); the British Columbia Knowledge Development Fund (BCKDF); the Mitacs Accelerate Program; the QuantEmX Program of the Institute for Complex Adaptive Matter; the Gordon and Betty Moore Foundation’s EPiQS Initiative, Grant GBMF4779 to A.D.; the Canada Research Chairs Program (A.D.); and the CIFAR Quantum Materials Program (A.D.). Use of the Canadian Light Source (Quantum Materials Spectroscopy Centre), a national research facility of the

University of Saskatchewan, is supported by CFI, NSERC, the National Research Council, the Canadian Institutes of Health Research, the Government of Saskatchewan and the University of Saskatchewan.

AUTHOR DECLARATIONS

Conflict of Interest

The authors have no conflicts to disclose.

Author Contributions

Chun Sum Brian Pang: Conceptualization (equal); Data curation (lead); Formal analysis (lead); Investigation (lead); Methodology (lead); Software (equal); Writing – original draft (lead); Writing – review and editing (lead). **Bruce A. Davidson:** Conceptualization (equal); Investigation (supporting); Methodology (supporting); Validation (equal); Writing – review and editing (equal). **Fengmiao Li:** Conceptualization (equal); Methodology (supporting). **Mohamed Oudah:** Investigation (supporting). **Peter Moen:** Investigation (supporting). **Steef Smit:** Investigation (supporting). **Cissy T. Suen:** Investigation (supporting). **Simon Godin:** Formal analysis (supporting); Software (equal). **Sergey A. Gorovikov:** Investigation (supporting). **Marta Zonno:** Investigation (supporting). **Sergey Zhdanovich:** Validation (equal). **Giorgio Levy:** Validation (equal). **Matteo Michiardi:** Validation (equal). **Alannah M. Hallas:** Supervision (supporting). **George A. Sawatzky:** Supervision (supporting); Validation (equal). **Robert J. Green:** Formal analysis (supporting); Software (equal); Validation (equal); Writing – review and editing (equal). **Andrea Damascelli:** Conceptualization (equal); Funding acquisition (equal); Project administration (equal); Resources (equal); Supervision (equal); Validation (equal); Writing – review and editing (equal). **Ke Zou:** Conceptualization (lead); Funding acquisition (equal); Project administration (equal); Resources (equal); Supervision (lead); Validation (equal); Writing – review and editing (equal).

DATA AVAILABILITY

The data that support the findings of this study are available from the corresponding author upon reasonable request.

REFERENCES

- ¹G. E. Jellison, I. Paulauskas, L. A. Boatner, and D. J. Singh, Phys. Rev. B **74**, 155130 (2006).
- ²P. D. C. King, R. H. He, T. Eknaphakul, P. Buaphet, S.-K. Mo, Y. Kaneko, S. Harashima, Y. Hikita, M. S. Bahramy, C. Bell, Z. Hussain, Y. Tokura, Z.-X. Shen, H. Y. Hwang, F. Baumberger, and W. Meevasana, Phys. Rev. Lett. **108**, 117602 (2012).

³A. F. Santander-Syro, C. Bareille, F. Fortuna, O. Copie, M. Gabay, F. Bertran, A. Taleb-Ibrahimi, P. Le Fèvre, G. Herranz, N. Reyren, M. Bibes, A. Barthélémy, P. Lecoeur, J. Guevara, and M. J. Rozenberg, Phys. Rev. B **86**, 121107 (2012).

⁴C. Bareille, F. Fortuna, T. C. Rödel, F. Bertran, M. Gabay, O. H. Cubelos, A. Taleb-Ibrahimi, P. Le Fèvre, M. Bibes, A. Barthélémy, T. Maroutian, P. Lecoeur, M. J. Rozenberg, and A. F. Santander-Syro, Sci. Rep. **4**, 3586 (2014).

⁵K. Zou, S. Ismail-Beigi, K. Kisslinger, X. Shen, D. Su, F. J. Walker, and C. H. Ahn, APL Mater. **3**, 036104 (2015).

⁶S. Mallik, G. C. Ménard, G. Saïz, H. Witt, J. Lesueur, A. Gloter, L. Benfatto, M. Bibes, and N. Bergeal, Nat. Commun. **13**, 4625 (2022).

⁷X. Chen, T. Yu, Y. Liu, Y. Sun, M. Lei, N. Guo, Y. Fan, X. Sun, M. Zhang, F. Alarab, V. N. Strocov, Y. Wang, T. Zhou, X. Liu, F. Lu, W. Liu, Y. Xie, R. Peng, H. Xu, and D. Feng, Nat. Commun. **15**, 7704 (2024).

⁸Y. Liu, Z. Liu, M. Zhang, Y. Sun, H. Tian, and Y. Xie, Chin. Phys. B **32**, 037305 (2023).

⁹A. Gupta, H. Silotia, A. Kumari, M. Dumen, S. Goyal, R. Tomar, N. Wadehra, P. Ayyub, and S. Chakraverty, Adv. Mater. **34**, 2106481 (2022).

¹⁰C. Liu, X. Yan, D. Jin, Y. Ma, H.-W. Hsiao, Y. Lin, T. M. Bretz-Sullivan, X. Zhou, J. Pearson, B. Fisher, J. S. Jiang, W. Han, J.-M. Zuo, J. Wen, D. D. Fong, J. Sun, H. Zhou, and A. Bhattacharya, Science **371**, 716 (2021).

¹¹L. F. Mattheiss, Phys. Rev. B **6**, 4718 (1972).

¹²L. M. Vicente-Arche, J. Bréhin, S. Varotto, M. Cosset-Cheneau, S. Mallik, R. Salazar, P. Noël, D. C. Vaz, F. Trier, S. Bhattacharya, A. Sander, P. Le Fèvre, F. Bertran, G. Saiz, G. Ménard, N. Bergeal, A. Barthélémy, H. Li, C.-C. Lin, D. E. Nikonorov, I. A. Young, J. E. Rault, L. Vila, J.-P. Attané, and M. Bibes, Adv. Mater. **33**, 2102102 (2021).

¹³S. Varotto, A. Johansson, B. Göbel, L. M. Vicente-Arche, S. Mallik, J. Bréhin, R. Salazar, F. Bertran, P. L. Fèvre, N. Bergeal, J. Rault, I. Mertig, and M. Bibes, Nat. Commun. **13**, 6165 (2022).

¹⁴A. H. Al-Tawhid, R. Sun, A. H. Comstock, D. P. Kumah, D. Sun, and K. Ahadi, Appl. Phys. Lett. **126**, 091601 (2025).

¹⁵X. Hua, F. Meng, Z. Huang, Z. Li, S. Wang, B. Ge, Z. Xiang, and X. Chen, npj Quantum Mater. **7**, 1 (2022).

¹⁶L. Chen, S. Zhou, D. Tian, Y. Xiao, Q. Gao, Y. Wang, Y. Chen, F. Hu, B. Shen, J. Sun, W. Zhao, J. Zhang, and H. Zhang, “Two-dimensional superconductivity at the CaZrO₃/KTaO₃ (001) heterointerfaces,” (2025), arXiv:2507.01392.

¹⁷C. Liu, X. Zhou, D. Hong, B. Fisher, H. Zheng, J. Pearson, J. S. Jiang, D. Jin, M. R. Norman, and A. Bhattacharya, Nat. Commun. **14**, 951 (2023).

¹⁸A. Alexander, M. Reticcioli, L. Albons, J. Redondo, M. Corrias, I. Příš, Z. Wang, V. Johánek, J. Mysliveček, C. Franchini, D. Wrana, and M. Setvin, ACS Appl. Mater. Interfaces **16**, 70010 (2024).

¹⁹A. Ichimura and P. I. Cohen, *Reflection High-Energy Electron Diffraction* (Cambridge University Press, Cambridge, 2004).

²⁰M. P. Seah and W. A. Dench, Surf. Interface Anal. **1**, 2 (1979).

²¹J. F. Moulder and J. Chastain, eds., *Handbook of X-ray photoelectron spectroscopy: a reference book of standard spectra for identification and interpretation of XPS data*, update ed. (Perkin-Elmer Corporation, Eden Prairie, Minn, 1992).

²²F. Y. Bruno, S. McKeown Walker, S. Riccò, A. de la Torre, Z. Wang, A. Tamai, T. K. Kim, M. Hoesch, M. S. Bahramy, and F. Baumberger, Adv. Electron. Mater. **5**, 1800860 (2019).

²³S. Mallik, B. Göbel, H. Witt, L. M. Vicente-Arche, S. Varotto, J. Bréhin, G. Ménard, G. Saïz, D. Tamsaout, A. F. Santander-Syro, F. Fortuna, F. Bertran, P. Le Fèvre, J. Rault, I. Boventer, I. Mertig, A. Barthélémy, N. Bergeal, A. Johansson, and M. Bibes, APL Mater. **11**, 121108 (2023).